Efficient oxide phosphors for light upconversion; green emission from Yb3+ and Ho3+ co-doped Ln(2)BaZnO(5) (Ln = Y, Gd)

Etchart, I; Hernandez, I; Huignard, A; Berard, M; Gillin, WP; Curry, RJ; Cheetham, AK

Efficient Oxide Phosphors for Light Upconversion; Green Emission from Yb^{3+} and Ho^{3+} Co-Doped Ln_2BaZnO_5 (Ln=Y, Gd)

Isabelle Etchart[ab], Ignacio Hernández[c], Arnaud Huignard[b], Mathieu Bérard[b], William. P. Gillin[c], Richard. J. Curry[d] and Anthony K. Cheetham[a]*

[a] *Materials Science and Metallurgy Department, University of Cambridge, Pembroke Street CB2 3QZ, UK*
[b] *Saint-Gobain Recherche, 39 quai Lucien Lefranc, 93303 Aubervilliers, France*
[c] *Department of Physics, Queen Mary University of London, Mile End Road, London, E1 4NS, UK*
[d] *Advanced Technology Institute, University of Surrey, Guildford, Surrey GU2 7XH, UK*

*Corresponding author: e-mail: akc30@cam.ac.uk

Abstract

The optical properties of Yb^{3+} and Ho^{3+} co-doped Y_2BaZnO_5, synthesized by solid-state reactions, are investigated in detail. Under 977 nm excitation (~ 25.10^{-3} W/mm^2), bright green upconversion emission is observed. Concentration dependence studies at room temperature show that relatively high infrared to visible upconversion efficiencies are obtained with values up to ~2.6 %. The results of power dependence studies and temperature dependent lifetime measurements allow us to determine the dominant upconversion mechanisms in Yb^{3+}: Ho^{3+} co-doped Y_2BaZnO_5 oxides. The materials presented in this paper constitute new and efficient upconversion phosphors which may find utility in a variety of applications.

1. Introduction

The upconversion luminescence properties of rare-earth doped materials for infrared to visible upconversion have been the focus of much research since the development, in the nineteen eighties, of cheap and high-powered InGaAs diode lasers emitting at around 980 nm.[i, ii, iii] Potential applications of these materials include biosensors,[iv, v, vi] colour displays[vii,viii,ix] and solar cells.[x,xi,xii,xiii] The idea of adding an upconversion material layer at the rear-face of a solar cell device is very attractive. This is particularly relevant to the area of organic solar cells, to which Prof Fred Wudl has contributed extensively.[xiv,xv] The upconverting material could help decrease the transmission losses of the solar-cell device by converting the sub-band gap infrared photons of the solar spectrum into visible photons that can be efficiently used by the solar cell. This requires the development of highly efficient and stable materials that can upconvert efficiently at the solar cell operating temperatures, with low excitation density thresholds.

Oxide materials are usually very stable chemically, mechanically, and thermally and could therefore be promising hosts for light upconversion applications. Ho^{3+} is an excellent dopant candidate for infrared to green upconversion because of its favourable intra-atomic 4*f* energy level structure. It has a relatively long-lived $^5I_7$ level that can act as a population reservoir for upconversion processes. Upconversion of Ho^{3+} has been widely reported under 650 nm,[xvi,xvii,xviii] 750 nm[xix,xx,xxi,xxii] and 875 nm[xxiii,xxiv] excitations, but often with poor efficiency. Higher upconversion efficiencies have been achieved in materials co-doped with Yb^{3+} and Ho^{3+}, where Yb^{3+} acts as a sensitizer for Ho^{3+} owing to its strong absorption around 980 nm.[xxv, xxvi] Oxides materials have been reported as suitable host for Ho^{3+} upconversion.[xxvii,xxviii]

In the present work, we present results obtained on a new upconversion material, namely Ln_2BaZnO_5: Yb^{3+}, Ho^{3+} (Ln=Y,Gd). Ln_2BaZnO_5 ternary oxide hosts were first reported by Raveau et al. in 1982.[xxix, xxx] Since then they have attracted attention for their interesting magnetic and optical properties. Ln_2BaMO_5 oxides (Ln = Y, Gd and M = Zn,

Cu) crystallize in the orthorhombic space group Pnma. Ln ions occupy two different sevenfold coordinated sites with the same symmetry but with slightly different Ln-O distances, while the M ions exhibit an unusual distorted tetrahedral coordination. Recently, the upconversion properties of $Y_2BaZnO_5:Yb^{3+},Er^{3+}$ and $Gd_2BaZnO_5:Yb^{3+},Er^{3+}$ under 980 nm continuous and pulsed excitation were investigated and bright green and red emissions observed.[xxxi,xxxii] In the present work, we focus on the investigation of Yb^{3+},Ho^{3+} co-doped Y_2BaZnO_5 for infrared to visible upconversion. We show that, by optimizing dopant concentrations, bright green upconversion luminescence can be achieved, with a relatively high efficiency of up to 2.6 %. Luminescence mechanisms are elucidated through power dependence studies and temperature dependant lifetime measurements on samples with different dopant concentrations.

2. Experimental

2.1. Synthesis of Y_2BaZnO_5: Yb^{3+}, Ho^{3+}phosphors

Y_2BaZnO_5: Yb^{3+}(x %), Ho^{3+}(y %) phosphors were synthesized by solid-state reactions. Stoichiometric amounts of Y_2O_3 (*Alfa Aesar*, 99.99 %), Yb_2O_3 (*Alfa Aesar*, 99.99 %), Ho_2O_3 (*Alfa Aesar*, 99.99%), ZnO (*Fisher Scientific*, 99.5 %) and $BaCO_3$ (*Fisher Scientific*, 99+ %) were mixed, ground together, and sintered at 1200°C for several days with intermediary grinding stages.

2.2. X-ray Powder Diffraction (XRPD) Analysis

X-ray powder diffraction patterns were measured using a theta-theta diffractometer (*Bruker* D8), equipped with a Cu Kα source (generator: 40 kV and 40 mA), a scintillation detector with pulse-height analysis, and a variable knife-edge collimator for high resolution X-ray diffractometry. The best achievable instrumental resolution is 0.08° in 2θ.

2.3. Upconversion Luminescence Spectroscopy

For emission spectra acquisition and upconversion efficiency measurements, the sample of interest was finely ground and sandwiched between two quartz plates (*Helma*, 106-QS), one of which was coated with a reflective film of silver. The sample holder was then placed at the rear face of an integrating sphere (*Instrument System*, ISP-150-100). For the acquisition of upconverted luminescence spectra, samples were excited using the 977 nm output of a temperature-controlled cw laser diode (*Thorlabs*, L980P100 and TCLDM9). The excitation signal was focused onto the centre of the sample holder using a lens (*Newport*, KPX049AR.16). After initial alignment of the setup, efficiency measurements were performed in two steps. For the first measurement, the quartz sample holder at the rear-face of the integrating sphere was left empty (no sample inside, rear-face silver coated), and the laser excitation on the sample was collected using an optical fibre and analyzed with a spectrometer (*Instrument System*, CAS 140B). From this measurement was determined the incident power in the near-infrared P_{inc}^{IR} (integrated over the 950-1000 nm range). It is worth noting that a previous calibration was performed for the integrating sphere with an undoped sample, to mimic the scattering, and no significant differences were found with respect to the empty sample holder with a reflective mirror at its rear. For the second measurement, the sample under investigation was placed inside the quartz holder, and both the fraction of the excitation light that had not been absorbed by the sample (power $P_{not\,abs}^{IR}$), and the emitted upconversion light in the 380-780 nm range (power P_{em}^{vis}), were collected and quantified. From these two measurements, the fraction of the incident power *absorbed* by the sample was calculated. The upconversion efficiency was calculated as the ratio of the upconverted emission in the range 380-780 nm to the power absorbed in the range 950-1000 nm:

$$\eta_{UC} = \frac{P_{em}^{vis}}{P_{abs}^{IR}} = \frac{P_{em}^{vis}}{P_{inc}^{IR} - P_{not\,abs}^{IR}}$$

A preliminary study showed that the statistical error on efficiency measurements (from repeated measurements) is of the order 6 %. The collected emission spectra in the 380-1000 nm range were corrected for instrumental response.

For emission rise-time and lifetime measurements, a tunable optical parametric oscillator (OPO) (*Continuum* Panther OPO) pumped by the third harmonic wavelength at 355 nm of a Q-switched YAG:Nd laser (*Surelite* I laser) was tuned to 455 nm or 977 nm to excite the sample with a 7 ns pulse at a 10 Hz repetition rate. The fluorescence from the sample was separated from the pumping light using a filter (*Schott*, GG 475), and was then passed through a spectrometer (*Jobin Yvon*, Triax 550) and detected using a photomultiplier tube detector (*Hamamatsu* R550) connected to a 500-MHz digital oscilloscope (*LeCroy*, 9350A) and a desktop computer. A continuous flow cryostat (*Oxford Instruments* Optistat and ITC) was used for low temperature measurements. For measurements above room temperature, a temperature controlled hot stage was used (*Linkam* THMS600 and TMS94).

3. Results

3.1. Crystal structure

Figure 1 shows the typical powder X-ray diffraction pattern of Y_2BaZnO_5:Yb^{3+}(7 %),Ho^{3+}(0.5 %). The crystal structure is orthorhombic, space group Pnma. Relatively pure phases are obtained, as shown by the good quality of the Rietveld refinement.[xxxiii] Cell parameters are: a=12.3387(1) A, b=5.70975(5) A and c=7.07037(7) A (ICDD 87082). Note that the lattice parameters obtained in the doped sample are slightly smaller than those in the pure phase, which is attributed to the smaller sizes of the Yb^{3+} (0.0925 nm) and Ho^{3+} (0.0958 nm) compared to Y^{3+} (0.096 nm).

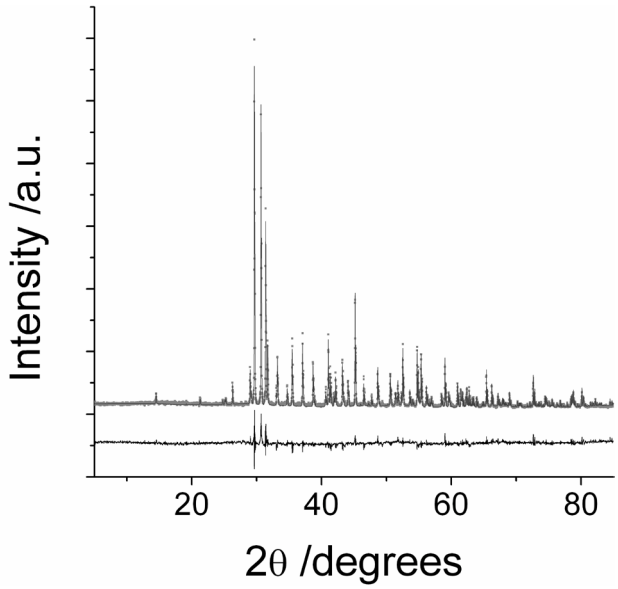

Figure 1: Rietveld refinement based upon X-ray powder diffraction pattern of Y_2BaZnO_5:Yb^{3+}(7 %),Ho^{3+}(0.5 %).

3.2. Upconversion luminescence emission

During 977nm excitation at room temperature, Y_2BaZnO_5:Yb^{3+},Ho^{3+} powders yield bright green emission, visible to the naked eye. Under 977 nm (corresponding to the selective excitation of Yb^{3+} $^2F_{5/2}$) and 455 nm excitation (selective excitation of Ho^{3+} $^3K_8$), typical emission spectra measurements reveal the presence of emission bands centred around 545 nm, 760 nm, 660 nm, 1040 nm (broad emission) and 1200 nm (Figure 2). A comparison of the emission spectra obtained under 977 nm and 455 nm excitation shows that the green (545 nm) to near-infrared (760 nm) emission intensity ratio does not vary with the excitation wavelength.

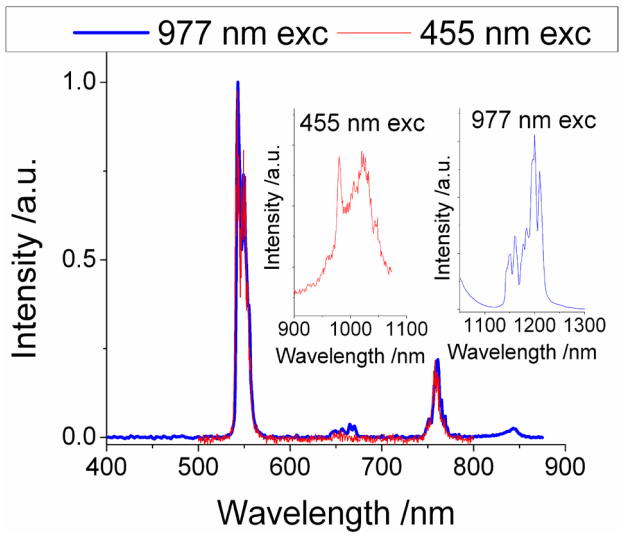

Figure 2: Typical luminescence spectra of $Y_2BaZnO_5:Yb^{3+},Ho^{3+}$ phosphors at room temperature under 977 nm and 455 nm excitations.

3.3. Concentration dependence of UC efficiencies

The upconverted emission intensity and spectral properties depend on the dopant concentrations. In Figure 3, the emission spectra of seven selected samples of the $Y_2BaZnO_5:Yb^{3+}$(x %),Ho^{3+}(0.5 %) (x = 1, 3, 5, 7, 9, 11, and 13) family are presented under cw 977 nm excitation (~ 36.10^{-3} W/mm^2 incident power). The upconversion emission intensity is seen to increase with the Yb^{3+} concentration, with an optimum performance around 5 % Yb^{3+}. When the Yb^{3+} concentration is increased above this value at constant Ho^{3+} concentration, the upconversion becomes less efficient. This can be explained by the appearance of concentration quenching, as has been observed in previous studies.[35] The inset of Figure 3 shows the evolution of the green (545 nm) to near-infrared (760 nm) emission intensity ratios for the same seven samples. For Yb^{3+} concentrations above ~3 %, the green to near-infrared ratio is seen to be constant with the Yb^{3+} concentration. A lower green to near-infrared ratio is measured on the sample doped with 1 % Yb^{3+}. In the second inset of Figure 3, the evolutions of green (545 nm) and red (660 nm) emission intensities with the Yb^{3+} concentration in the same seven samples are represented. The green emission intensities increase strongly with increasing Yb^{3+}

concentration before reaching a maximum around 5 % Yb^{3+}. For higher Yb^{3+} concentrations, the green emission intensity decreases with increasing Yb^{3+} concentration. The near-infrared emission intensities present the same dependence on Yb^{3+} concentration as the green emission intensities for Yb^{3+} concentrations above ~3 %. The red emission intensity is shown to increase very slightly with Yb^{3+} concentration.

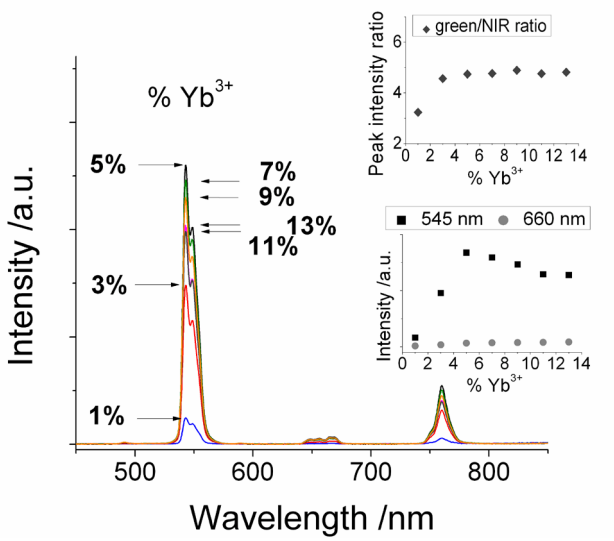

Figure 3: Upconversion luminescence spectra for seven samples of the $Y_2BaZnO_5:Yb^{3+}$(x %), Ho^{3+}(0.5 %) (x = 1, 3, 5, 7, 9, 11, and 13) family at room temperature under 977 nm cw excitation. The insets present the evolutions of the green (545 nm) to near-infrared (760 nm) intensity ratio (top inset) and of the green (545 nm) and red (660 nm) emission intensities (bottom inset) as a function of Yb^{3+} concentration under cw 977 nm excitation (~ 36.10^{-3} W/mm^2 incident power).

The upconversion efficiencies of a variety of $Y_2BaZnO_5:Yb^{3+}$(x %),Ho^{3+}(y %) samples ($0 \leq x \leq 15$ and $0 \leq y \leq 3$) were measured at room temperature under 977 nm excitation (~ 25.10^{-3} W/mm^2 incident power) (Figure 4 and Figure S1, supplementary information). Samples containing between 0.25 - 0.75 % of Ho^{3+}, and total dopant concentrations (Yb^{3+} plus Ho^{3+}) in the 5 - 9 % range were shown to exhibit the highest efficiencies for infrared to visible upconversion. A maximum upconversion efficiency of 2.6 ± 0.2 % was

obtained with $Y_2BaZnO_5:Yb^{3+}$(7 %),Ho^{3+}(0.5 %) at room temperature under ~ 25.10^{-3} W/mm^2 excitation. It is worth noting that very similar upconversion efficiency values (and behaviour) were obtained from $Gd_2BaZnO_5:Yb^{3+},Ho^{3+}$ samples.

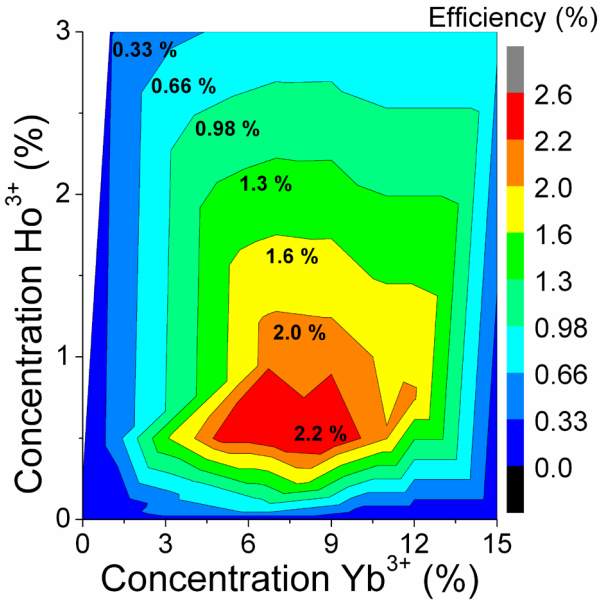

Figure 4: Room temperature upconversion efficiencies as a function of dopant concentration for a variety of $Y_2BaZnO_5:Yb^{3+},Ho^{3+}$ samples. The colour bar on the right is used to display the upconversion efficiency values for each dopant composition. Contour lines (lines with the same upconversion efficiency value) and contour labels displaying the UC efficiencies associated to those contour lines are also included.

3.4. Pump power dependence of the luminescence emission

Pump power dependences of the green (545 nm), near-infrared (760 nm) and red (660 nm) emissions were investigated at room temperature under 977 nm excitation. The three emissions were shown to present an approximate quadratic dependence on the excitation power density in the low power regime (Figure 5). It is worth mentioning that for ~ 25.10^{-3} W/mm^2 excitation densities, about half of the incident light on the sample is absorbed, i.e. $P^{IR}_{not\ abs} \sim \frac{1}{2} P^{IR}_{inc}$.

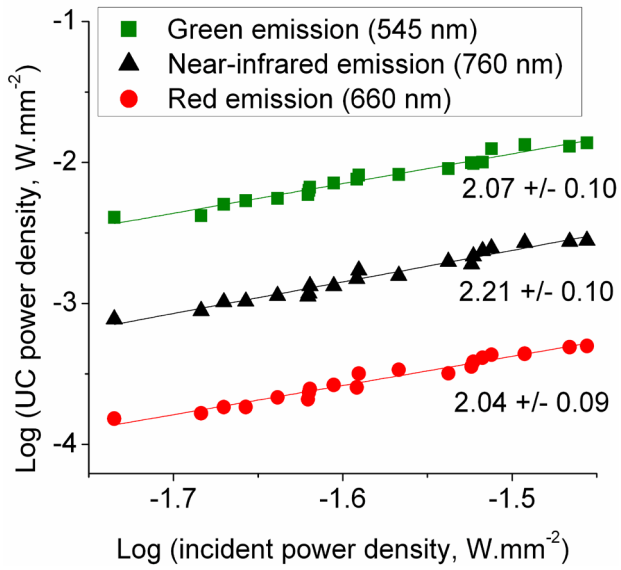

Figure 5: Pump power density dependence of the green (545 nm), red (660 nm) and near-infrared (760 nm) upconversion (UC) emission at room temperature under 977 nm excitation in Y_2BaZnO_5: Yb^{3+} (7 %), Ho^{3+} (0.5 %). The results are presented in a decadic double-logarithmic scale.

3.5. Lifetime measurements, temperature dependence

The temporal evolutions of the emissions centred at around 545 nm, 760 nm, 1040 nm, and 1200 nm in Y_2BaZnO_5:Yb^{3+}(7 %), Ho^{3+}(0.5 %) were recorded under pulsed 455 nm (direct excitation of Ho^{3+} $^3K_8$) and 977 nm (excitation of Yb^{3+} $^2F_{5/2}$) in the 80 K -573 K range. It is worth noting that Ho^{3+} does not absorb at 977 nm, which guarantees a selective excitation of Yb^{3+} under 977 nm excitation. A typical transient corresponding to the room temperature temporal evolution of the green emission (545 nm) under pulsed 977 nm excitation in Y_2BaZnO_5: Yb^{3+}(7 %), Ho^{3+}(0.5 %) is presented in Figure 6. At the end of the excitation pulse ($t \approx 0$), no luminescence intensity is observed; instead, the transient exhibits a typical delayed rise and a decay. This is a clear fingerprint of an energy transfer process. The experimental intensity data were fitted to the expression:[xxxiv]

$$I(t) = A\left(1 - e^{-\frac{t}{\tau_r}}\right)\left(e^{-\frac{t}{\tau_d}}\right) \qquad (1)$$

where A is an emission intensity factor, and τ_r and τ_d represent the rise and decay times of the transient. Note that τ_r and τ_d are related to the transfer rate constants between Yb^{3+} and Ho^{3+} and to the intrinsic lifetimes of the levels involved.[xxxiv] The decay curves showed, in some cases bi- or triexpontial behaviour, corresponding to decay mechanisms via different depopulation channels. As such, when the transient decay section could not be fitted by a single exponential, the effective fluorescent decay time τ_d was determined using the following equation (discretisation of the formula used in reference [xxxv]).

$$\tau_d = \frac{\sum_{i=1}^{n} A_i \tau_i^2}{\sum_{i=1}^{n} A_i \tau_i} \qquad (2)$$

where A_i and τ_i are the amplitude and lifetime corresponding to the level depopulation channel i, respectively, and n = 1, 2 or 3.

The fit of the typical room temperature transient corresponding to the green emission (545 nm) under pulsed 977 nm excitation of the Y_2BaZnO_5: Yb^{3+}(7 %), Ho^{3+}(0.5 %) sample is presented in Figure 6. The transient decay function presents two distinct lifetimes. The best fit for the 545 nm emission transient corresponds to average rise and decay times of τ_r = 14.4 ± 0.72 μs and τ_d = 280 ± 14 μs.

It is worth noting that for given dopant concentrations, the lifetimes measured under 977 nm excitation are longer than those obtained under direct 455 nm excitation (Figure 7b).[xxxvi] Moreover, for Yb^{3+} concentrations above ~3 %, the transients corresponding to the green (545 nm) and near-infrared (760 nm) emissions present the same rise and decay times (within experimental errors) in the whole range of temperatures studied (Figure 7b).

Figure 6: Typical temporal evolution of the green (545 nm) emission under pulsed 977 nm excitation and data fitting in order to get average rise and decay times in Y_2BaZnO_5:

Yb^{3+}(7 %), Ho^{3+}(0.5 %) at room temperature. Note that the small peak observed at around t ~ -140 μs is due to a triggering artefact. The inset presents an expansion of the initial rise.

In Figure 7, the temperature dependence of the lifetimes corresponding to *(a)* the broad 1040 nm emission from Yb^{3+} under 900 nm excitation, *(b)* the 545 nm green and 760 nm near-infrared emissions from Ho^{3+} under 977 nm and 455 nm excitations, and *(c)* the 1200 nm emission from Ho^{3+} under 977 nm and 455 nm excitations in Y_2BaZnO_5: Yb^{3+} (7 %), Ho^{3+} (0.5 %) are shown. For clarity, the error bars are not shown in Figure 7a, 7b and 7c but are typically of the order 5 % (statistical error on repeated measurements).

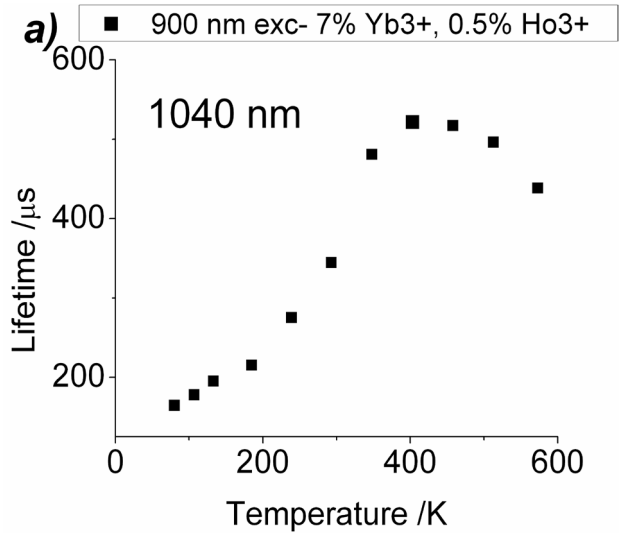

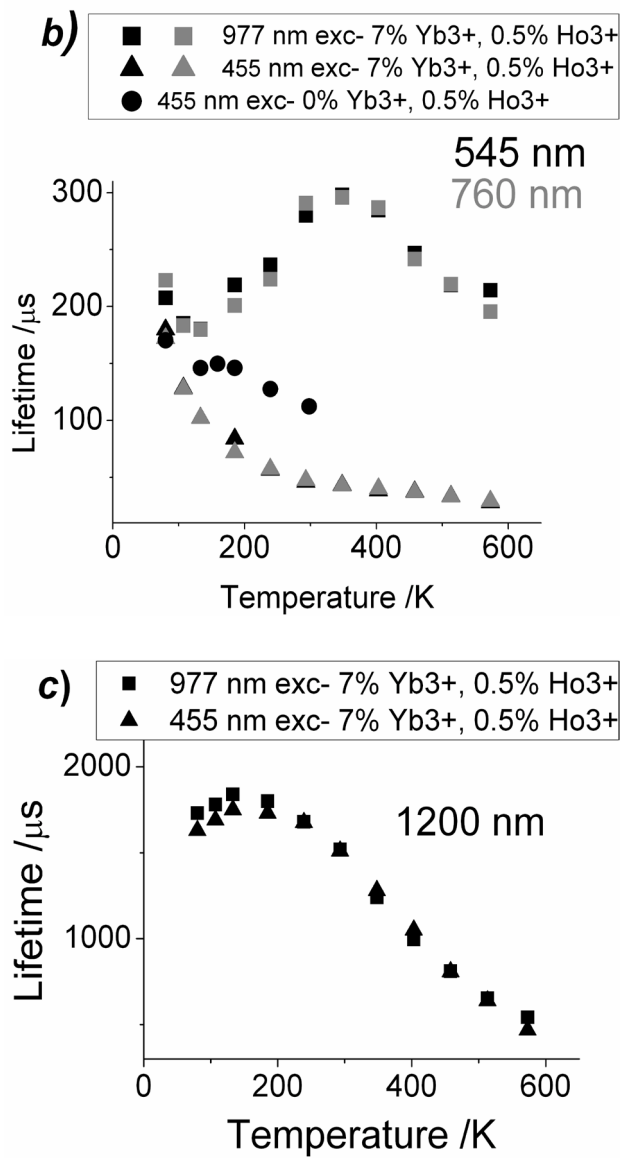

Figure 7: Temperature dependence in Y_2BaZnO_5:Yb^{3+}(7 %),Ho^{3+}(0.5 %) of the lifetimes corresponding to *a)* the 1040 nm emission under pulsed 900 nm excitation, *b)* the 545 nm green and 760 nm near-infrared emissions under pulsed 977 nm and 455 nm excitations, *c)* the 1200 nm emission under pulsed 977 nm and 455 nm excitations. Note that in graph *b),* the temperature dependence (up to room temperature) of the 545 nm green emission lifetime in a Y_2BaZnO_5:Yb^{3+}(0 %),Ho^{3+}(0.5 %) sample (no Yb^{3+}) under pulsed 455 nm

excitation is also represented for comparison. No data was recorded above room temperature.

Under 900 nm excitation (Figure 7a), the lifetime corresponding to the broad emission around 1040 nm increases with increasing temperature, $\tau_d^{\sim}$ 165 ± 8 μs at T = 80 K to $\tau_d^{\sim}$ 522 ± 26 μs at T = 403 K, when it saturates. At temperatures above 405 K, the lifetime decreases again reaching $\tau_d^{\sim}$ 438 ± 22 μs at T = 573 K (Table S1, supplementary information).

As shown in Figure 7b, the Y_2BaZnO_5:Yb^{3+}(7 %), Ho^{3+} (0.5 %) 545 nm and 760 nm emission lifetimes corresponding to the 545 nm and 760 nm emissions presents very different temperature dependences under 977 nm and 455 nm excitations. Under 977 nm excitation, corresponding to the selective excitation of Yb^{3+} $^2F_{5/2}$, the 545 nm and 760 nm emission upconversion lifetimes decrease with decreasing temperature for T < 350 K and reach a minimum of $\tau_d^{UC}{}_{\sim}$ 179 ± 9 μs at T = 130 K, before slightly increasing at lower temperatures up to τ_d^{UC} ~215 ± 11 μs at T = 80 K (average of the 545 nm and 760 nm emission lifetimes). For T > 350 K, the green emission lifetime decreases with increasing temperature, from $\tau_d^{UC}{}_{\sim}$ 300 ± 15 μs at T = 350 K to $\tau_d^{UC}{}_{\sim}$ 204 ± 10 μs at T = 573 K. On the other hand, under 455 nm direct excitation of Ho^{3+} $^3K_8$, the green emission lifetime decreases monotonically with increasing temperature (this is the case in the whole range of temperatures studied) from $\tau_d^{direct}{}_{\sim}$ 182 ± 9 μs at T = 80 K to $\tau_d^{direct}{}_{\sim}$ 30 ± 1.5 μs at T = 573 K. It is worth noting that, for the 7 % Yb^{3+}, 0.5 % Ho^{3+} sample, the lifetimes corresponding to the green emission (545 nm) measured under 977 nm and 455 nm excitations are similar at temperatures around 80 K. For increasing temperatures in the 80-400 K range, the two graphs plotting the temperature dependences of lifetimes under both excitation wavelengths diverge. Note that the lifetimes measured under 977 nm excitation are always longer than those measured under 455 nm excitation.[xxxvii] Figure 7b also shows the temperature dependence of the green emission lifetimes under 455 nm excitation in a purely Ho^{3+} doped

Y_2BaZnO_5:Yb^{3+}(0 %),Ho^{3+}(0.5 %) sample. Lifetimes measured in this Yb^{3+}-free sample under 455 nm are seen to decrease with temperature, from $\tau_d^{direct}{}_{\sim}$ 170 ± 9 µs at T = 80 K to $\tau_d^{direct}{}_{\sim}$ 112 ± 6 µs at T = 300 K similarly to what observed in Y_2BaZnO_5:Yb^{3+}(7 %),Ho^{3+}(0.5 %). However, for a given temperature, the lifetimes measured in the Yb^{3+}-free sample are always higher than those measured in the Yb^{3+}, Ho^{3+} co-doped sample. Note that the three graphs plotted in Figure 7b tend to almost converge for T = 80 K.

The temperature dependence of the 1200 nm emission under 977 nm and 455 nm excitations is represented in Figure 7c. The lifetimes measured under 977 nm and 455 nm excitations are almost identical for temperatures above 220 K, but show a slight deviation at low temperatures. In the whole temperature range (and especially at low temperatures), the lifetimes of the 1200 nm emission are very long. For T > 185 K, the 1200 nm emission lifetimes measured under both 977 and 455 nm excitations decay strongly with increasing temperature; $\tau_d^{455\ nm}$ ~ 1730 ± 87 µs, $\tau_d^{977\ nm}$ ~ 1800 ± 90 µs (T = 185 K) down to τ_d^{direct} ~ 469 ± 23 µs, τ_d^{UC} ~ 544 ± 27 µs (T = 573 K). For T < 185 K, the measured lifetimes decrease slightly with decreasing temperature; τ_d^{direct} ~ 1730 ± 87 µs, τ_d^{UC} ~ 1800 ± 90 µs (T = 185 K), τ_d^{direct} ~1630 ± 81 µs, τ_d^{UC} ~ 1730 ± 87 µs (T = 80 K).

4. Discussion

Population and depopulation mechanisms of the energy levels of interest

A detailed investigation of the steady-state and dynamic emission properties of a variety of Y_2BaZnO_5:Yb^{3+}(x %),Ho^{3+}(y %) ($0 < x \leq 3$ and $0 < y \leq 15$) samples was performed and the results were presented in the previous section.

Under 977 nm Yb^{3+} excitation, the samples present a strong green upconversion emission, easily visible to the naked eye. Maximum upconversion efficiencies of ~2.6 % are obtained at room temperature on samples doped with Yb^{3+} and Ho^{3+} concentrations around 7 % and 0.5 %, respectively (Figure 4). The emission spectra measurements reveal the presence of emission bands centred around 545 nm (strong upconversion emission), 660 nm (weak upconversion emission), 760 nm, 1040 nm (strong and broad emission) and 1200 nm (strong and broad emission). Under 977 nm excitation, the transients corresponding to the emissions centred at 545 nm, 760 nm and 1200 nm present a clear rise time after the excitation is turned off, indicating that the population mechanisms of the energy levels from which these emissions arise involve at least one Yb^{3+} to Ho^{3+} energy transfer step (Figure 6). Power dependence studies show that under 977 nm excitation the emission centred around 545 nm, 760 nm and 660 nm present a quadratic dependence on the excitation power, indicating a two-photon population process of their emitting levels (Figure 5). According to the energy diagram (Figure 8), the emissions centred at 545 nm, 660 nm, 1200 nm and 1040 nm can be assigned to the Ho^{3+} ($^5S_2$,$^5F_4$) → $^5I_8$, Ho^{3+} $^5F_5$ → $^5I_8$, Ho^{3+} $^5I_6$ → $^5I_8$ and Yb^{3+} $^2F_{5/2}$ → $^2F_{7/2}$ transitions, respectively. The near infrared emission centred at around 760 nm could be attributed to the Ho^{3+} $^5I_4$ → $^5I_8$ [30] and/or Ho^{3+} ($^5S_2$,$^5F_4$) → $^5I_7$ transitions.[xxvi,xxxvii,xxxviii] The invariance of the green (545 nm) to near-infrared (760 nm) emission intensity ratio with the excitation wavelength (Figure 2), and with Yb^{3+} concentration (for Yb^{3+} concentrations above 3 %, Figure 3), suggests that both the 545 nm and 760 nm emissions might arise from the same Ho^{3+} level, in this case the thermalized Ho^{3+} ($^5S_2$,$^5F_4$) levels. This is confirmed by the comparison of the transients corresponding to the 545 nm and 760 nm emissions (Figure 7b); the rise and decay times corresponding to these two emissions are very similar (within experimental errors) over the whole temperature range that was investigated. In view of these results, the emission centred at 760 nm can be exclusively assigned to the ($^5S_2$,$^5F_4$) → $^5I_7$ transition. Note that a surprisingly low green to near-infrared ratio was observed on the sample doped with 1 % Yb^{3+} (Figure 3). A possible explanation to this low value could be the existence of an additional channel for the 760 nm emission in addition to the ($^5S_2$,$^5F_4$) → $^5I_7$ emission, possibly via a Ho^{3+} $^5I_4$ → $^5I_8$

depopulation.[30] This fact, together with a significantly decreased green to red upconversion emission ratio for Yb^{3+} concentrations smaller than 3 %, suggests that processes involving an excited state absorption (ESA) from the long lived $^5I_7$ Ho^{3+} state could be relevant at low Yb^{3+} concentrations a reduced energy transfer upconversion (ETU) probability.

Figure 8: Simplified energy level diagram of Ho^{3+} and Yb^{3+} ions and the dominant upconversion mechanisms in Y_2BaZnO_5:Yb^{3+},Ho^{3+}. Radiative processes of ground state absorption (GSA), excited state absorption (ESA) and green, red and near-infrared luminescence, as well as non-radiative energy transfer upconversion (ETU), back energy transfer (BET) and multiphonon relaxation processes, are represented.

According to the energy diagram (Figure 8), one can see two different ways of populating the thermalized ($^5S_2$,$^5F_4$) energy levels. The first mechanism involves two successive Yb^{3+} to Ho^{3+} energy transfer steps; Yb^{3+} $^2F_{5/2}$ + Ho^{3+} $^5I_8$ → Yb^{3+} $^2F_{7/2}$ + Ho^{3+} $^5I_6$ and Yb^{3+} $^2F_{5/2}$ + Ho^{3+} $^5I_6$ → Yb^{3+} $^2F_{7/2}$ + Ho^{3+} ($^5S_2$,$^5F_4$). Alternatively, the ($^5S_2$,$^5F_4$) levels could be populated by a first Yb^{3+} to Ho^{3+} energy transfer step: Yb^{3+} $^2F_{5/2}$ + Ho^{3+} $^5I_8$ → Yb^{3+} $^2F_{7/2}$ + Ho^{3+} $^5I_6$ followed by an excited state absorption (ESA) by Ho^{3+} $^5I_6$ (with no Yb^{3+} assistance). However, given the high absorption cross-section of Yb^{3+} at 977 nm[xxxix] compared to that of Ho^{3+},[xl,xli,xlii] and the relatively high Yb^{3+} to Ho^{3+} concentration ratios in the samples, the first mechanism involving two successive Yb^{3+} to Ho^{3+} energy transfers is expected to be dominant in the population process for Ho^{3+} ($^5S_2$,$^5F_4$) for moderate and high relative Yb^{3+} concentrations.

Inspection of the energy diagram reveals three possible ways of populating the red emitting Ho^{3+} $^5F_5$ level. First, it could be populated by multiphonon relaxation from the above lying green emitting levels; ($^5S_2$,$^5F_4$) → $^5F_5$. The second mechanism involves a phonon-assisted Yb^{3+} to Ho^{3+} energy transfer: Yb^{3+} $^2F_{5/2}$ + Ho^{3+} $^5I_8$ → Yb^{3+} $^2F_{7/2}$ + Ho^{3+} $^5I_6$, followed by a multiphonon relaxation step to the long lived Ho^{3+} $^5I_7$ level: $^5I_6$ → $^5I_7$

and a second Yb^{3+} to Ho^{3+} energy transfer step populating directly the Ho^{3+} $^5F_5$ red emitting level: Yb^{3+} $^2F_{5/2}$ + Ho^{3+} $^5I_7$ → Yb^{3+} $^2F_{7/2}$ + Ho^{3+} $^5F_5$. Alternatively, the second Yb^{3+} $^2F_{5/2}$ to Ho^{3+} $^5I_7$ energy transfer step could be replaced by an excited state absorption (ESA) by Ho^{3+} $^5I_7$. Again, given the high absorption cross-section of Yb^{3+} at 977 nm compared to that of Ho^{3+},and the relatively high Yb^{3+} to Ho^{3+} concentration ratios in the samples, the mechanism involving two successive Yb^{3+} to Ho^{3+} energy transfers is expected to be dominant in the population process for Ho^{3+} $^5F_5$.

Ytterbium concentration dependence studies of the emission properties of Y_2BaZnO_5:Yb^{3+}(x %),Ho^{3+}(0.5 %) (x = 1, 3, 5, 7, 9, and 11) samples (inset Figure 3) show that for Yb^{3+} concentrations below 5 %, green (545 nm) and near infrared (760 nm) emission intensities increase with increasing Yb^{3+} concentration. This can be attributed to an increase in Ho^{3+} ($^5S_2$,$^5F_4$) population due to an increased Yb^{3+} sensitization. Lifetime measurements show that under 977 nm excitation, the ($^5S_2$,$^5F_4$) level lifetime decreases with increasing Yb^{3+} concentration (for Yb^{3+} concentrations ranging from 3 % to 11 %). This indicates that there is an additional process that depopulates the ($^5S_2$,$^5F_4$) level in the presence of Yb^{3+} ions that is more favourable at high Yb^{3+} concentrations. It is worth mentioning that multiphonon relaxation rates are not expected to be dependent on dopant concentrations, and in particular Yb^{3+} concentrations since the phonon energy is quasi-invariant at these low doping levels (Figure S2, supplementary information). The Yb^{3+} concentration dependent depopulation of Ho^{3+} ($^5S_2$,$^5F_4$) could be attributed to a back-energy transfer mechanism between Ho^{3+} and Yb^{3+}: Ho^{3+} ($^5S_2$,$^5F_4$) + Yb^{3+} $^2F_{7/2}$ → Ho^{3+} $^5I_6$ + Yb^{3+} $^2F_{5/2}$.[xliii,xliv,xlv] Energy transfer from Ho^{3+} to Yb^{3+} does exist, as evidenced by the broad emission attributed to Yb^{3+} $^2F_{5/2}$ → $^2F_{7/2}$ under selective excitation of Ho^{3+} at 455 nm (Figure 2).

The increase in the green and infrared (760 nm) emission intensities for Yb^{3+} concentrations below 5 % indicates that, in this concentration range, the ($^5S_2$,$^5F_4$) levels become more populated by Yb^{3+} to Ho^{3+} energy transfer than they are depopulated by Ho^{3+} to Yb^{3+} back-energy transfer. For Yb^{3+} concentrations below 5 %, the red emission intensity also increases slightly. This indicates that the higher the Yb^{3+} concentration, the

higher the ratio between Ho^{3+} $^5F_5$ population and Ho^{3+} $^5F_5$ depopulation. When the Yb^{3+} concentration exceeds 5 %, the green emission intensity starts decreasing with increasing Yb^{3+} concentration. This means that the higher the Yb^{3+} concentration, the higher the influence of Ho^{3+} to Yb^{3+} back-energy transfer (depopulating Ho^{3+} ($^5S_2$,$^5F_4$)) compared to that of the Yb^{3+} to Ho^{3+} energy transfer route populating Ho^{3+} ($^5S_2$,$^5F_4$). In this same Yb^{3+} concentration range, the red emission intensity keeps increasing slightly despite the decrease in green level population (Figure 3). Moreover, a comparison of the emission spectra measured under 977 nm and 455 nm excitations shows that the Ho^{3+} $^5F_5$ level emission is enhanced in the upconversion spectrum (as evidenced by the lower green to red emission intensity ratio) (Figure 2). This indicates that Ho^{3+} ($^5S_2$,$^5F_4$) → $^5F_5$ multiphonon relaxation is not the only process populating Ho^{3+} $^5F_5$ under 980 nm excitation. Yb^{3+} to Ho^{3+} $^5I_7$ energy transfer cannot be neglected when considering the population mechanisms of Ho^{3+} $^5F_5$; the increase in red emission can be attributed to an increase of the Yb^{3+} to Ho^{3+} $^5I_7$ energy transfer rates with Yb^{3+} concentration. The importance of this red level population channel involving Ho^{3+} $^5I_7$ is confirmed by the observation of the transients corresponding to the emissions at 545 nm, 760 nm and 660 nm (Figure S3, supplementary information). Both the green and near-infrared (760 nm) emissions are seen to present the same rise time; the red (660 nm) emission, however, presents a different average rise time, which is shorter. This suggests that the main population mechanism of the red emitting level upconversion is not multiphonon relaxation from Ho^{3+} ($^5S_2$,$^5F_4$) since this would lead to longer rise times of the red level compared to that associated to the 545 nm and 760 nm emissions. These results confirm that the contribution of Yb^{3+} to Ho^{3+} energy transfer: Yb^{3+} $^2F_{5/2}$ + Ho^{3+} $^5I_7$ → Yb^{3+} $^2F_{7/2}$ + Ho^{3+} $^5F_5$ to the population of Ho^{3+} $^5F_5$ cannot be neglected.

Population and depopulation dynamics as a function of temperature:

Temperature dependence studies of the Yb^{3+} $^2F_{5/2}$ lifetimes under direct 900 nm excitation (observation of the transient corresponding to the broad emission around 1040 nm emission) in Y_2BaZnO_5:Yb^{3+}(7 %),Ho^{3+}(0.5 %) show that the maximum lifetimes are

at around 420 K and decrease strongly with decreasing temperature down to 80 K, which is the limit of our measurements (Figure 7a). One can see three major ways of depopulating the Yb^{3+} $^2F_{5/2}$ level; the first process involves Yb^{3+} to Ho^{3+} energy transfer (three different transfer processes must be considered: Yb^{3+} $^2F_{5/2}$ + Ho^{3+} $^5I_8$ → Yb^{3+} $^2F_{7/2}$ + Ho^{3+} $^5I_6$; Yb^{3+} $^2F_{5/2}$ + Ho^{3+} $^5I_6$ → Yb^{3+} $^2F_{7/2}$ + Ho^{3+} ($^5S_2$,$^5F_4$); and Yb^{3+} $^2F_{5/2}$ + Ho^{3+} $^5I_7$ → Yb^{3+} $^2F_{7/2}$ + Ho^{3+} $^5F_5$). The second process would involve Yb^{3+} $^2F_{5/2}$ → $^2F_{7/2}$ multiphonon relaxation, but in view of the large energy gap between the Yb^{3+} ground and excited states (~ 10400 cm^{-1}), the rates of multiphonon relaxation are expected to be low. We have observed that excitation hopping between Yb^{3+} does not contribute significantly to the Yb^{3+} $^2F_{5/2}$ lifetime, as no significant concentration dependence has been found with the Yb^{3+} concentration in singly doped samples. Besides, the temperature dependence of the Yb^{3+} $^2F_{5/2}$ lifetimes observed in Figure 7a is very different from that expected for a process governed by multiphonon relaxation[xlvi] so we conclude that for T < 420 K, the decrease of lifetimes with decreasing temperature reflects the increase in the global Yb^{3+} to Ho^{3+} transfer rate (which includes three contributions corresponding to the transfers to Ho^{3+} $^5I_8$, Ho^{3+} $^5I_6$ and Ho^{3+} $^5I_7$). This increase can be assigned to an improved overlap between the emission from Yb^{3+} emission and any of the absorptions by Ho^{3+} $^5I_8$, Ho^{3+} $^5I_6$ and/or Ho^{3+} $^5I_8$. The remarkable increase of the green upconversion intensity supports this idea and suggests that the resonant transfer to Ho^{3+} $^5I_6$ is the main beneficiary of this transfer probability increase.

Temperature dependence studies of the Ho^{3+} $^5I_6$ lifetimes in Y_2BaZnO_5:Yb^{3+}(7 %),Ho^{3+}(0.5 %) (observation of the temporal evolution of the 1200 nm emission) show that for T > 200 K, the Ho^{3+} $^5I_6$ lifetimes measured under 977 nm and 455 nm excitation are very similar and decrease with increasing temperature (Figure 7c). The Ho^{3+} $^5I_6$ level can be depopulated either by multiphonon relaxation to Ho^{3+} $^5I_7$, by Yb^{3+} to Ho^{3+} ET: Yb^{3+} $^2F_{5/2}$ + Ho^{3+} $^5I_6$ → Yb^{3+} $^2F_{7/2}$ + Ho^{3+} ($^5S_2$,$^5F_4$), or by phonon-assisted Ho^{3+} to Yb^{3+} back-energy transfer. This suggests that the Ho^{3+} $^5I_6$ dynamics might be governed mainly by the Ho^{3+}, and in particular by the Ho^{3+} $^5I_6$ → $^5I_7$ multiphonon relaxation rate, which is expected to increase with temperature (the Ho^{3+} $^5I_6$ lifetime is not governed by Yb^{3+} - Ho^{3+} interaction dynamics). The slight lifetime

decrease (of around 100 μs for $\tau_d^{455\,nm}$ and 70 μs for $\tau_d^{977\,nm}$) in the 185 K - 80 K range suggests that, despite the low Ho^{3+} concentrations in the samples, cross-relaxation mechanisms involving the lowest excited states of Ho^{3+} occur at low temperatures. These mechanisms are weak and only possible due to the long lifetimes of the levels involved.[xlvii]

The temperature dependence study of the temporal evolution of the Ho^{3+} green emission at 545 nm in Y_2BaZnO_5:Yb^{3+}(7 %),Ho^{3+}(0.5 %) shows that the thermal behaviour is completely different under 455 nm excitation (down-conversion by selective excitation of Ho^{3+} $^3K_8$) compared with that under 977 nm excitation (upconversion through selective excitation of Yb^{3+} $^2F_{5/2}$) (Figure 7c). Interestingly, the lifetimes measured under 977 nm excitation are longer than those measured under 455 nm excitation, for T > 80 K. This is a clear indication that the upconversion dynamics are governed by the Yb^{3+}- Ho^{3+} interaction dynamics and not by the intrinsic Ho^{3+}($^5S_2$,$^5F_4$) lifetimes.[xlviii] Under 455 nm excitation, the strong decrease of Ho^{3+} ($^5S_2$,$^5F_4$) lifetimes with increasing temperature (Figure 7c) suggests that Ho^{3+} ($^5S_2$,$^5F_4$) → $^5F_5$ multiphonon relaxation governs the green and near-infrared (760 nm) emitting level depopulation dynamics. A comparison of the lifetimes in Y_2BaZnO_5:Yb^{3+}(7 %),Ho^{3+}(0.5 %) and Y_2BaZnO_5:Yb^{3+}(0 %),Ho^{3+}(0.5 %) under 455 nm excitation shows that, for each temperature, the sample containing Yb^{3+} (7 %) presents lower intrinsic lifetimes than the Yb^{3+} free sample. This indicates that Ho^{3+} to Yb^{3+} back-energy transfer does exist, even under 455 nm excitation. At high temperatures, its contribution, however, is low compared to that of ($^5S_2$,$^5F_4$) → $^5F_5$ multiphonon relaxation. Under 977 nm excitation, a distinct behaviour of Ho^{3+} ($^5S_2$,$^5F_4$) emission is observed, the lifetime decreasing with decreasing temperature.

The lifetimes measured under 977 nm and 455 nm excitation tend to (almost) converge. This observation is noteworthy, and suggests that there is a change in the dynamics regime at low temperatures; the system is no longer governed by Yb^{3+}-Ho^{3+} transfer times but by Ho^{3+} ($^5S_2$,$^5F_4$) → $^5F_5$ intrinsic de-excitation times. We believe that this paper constitutes the first report of a dynamics regime change by means of temperature variation in a Yb^{3+},Ho^{3+} doped system. A more elaborated theoretical study of

temperature-dependent upconversion dynamics (rate equation solving, Monte Carlo simulation) is in progress and should allow us to get a better understanding of the change in dynamics regime experimentally observed.

The relevant upconversion mechanisms for $Ln_2BaZnO_5:Yb^{3+},Ho^{3+}$ are summarized in Figure 8.

5. Conclusions and future work

A very efficient near-infrared to green upconversion phosphor is presented in this paper. Upconversion properties of $Y_2BaZnO_5:Yb^{3+},Ho^{3+}$ oxide materials were investigated as a function of dopant concentration and their upconversion efficiencies quantified. We believe that the high upconversion efficiencies obtained at room temperature (~2.5 %) are the highest reported to date for an Yb^{3+}, Ho^{3+} co-doped oxide phosphor.

Power dependence studies and temperature dependent lifetime measurements provide a model for the upconversion mechanisms involved in these materials. The strong green (545 nm) and near-infrared (760 nm) emissions arise from the thermalised Ho^{3+} ($^5S_2$,$^5F_4$) levels populated mainly by two successive Yb^{3+} to Ho^{3+} energy transfer steps under 977 nm excitation. Temperature-dependent lifetime studies suggest that there is an interesting change in upconversion dynamics occurring at low temperatures in $Y_2BaZnO_5:Yb^{3+}$(7 %),Ho^{3+}(0.5 %).

Acknowledgments

This work was supported by the Saint-Gobain Recherche Company, France. IH acknowledges support by and the Royal Academy of Engineering/EPSRC. We gratefully thank Olivier Delrieu and Marine Laroche for useful discussions and assistance in efficiency measurements.

References

[i] F. Auzel, *F.C.R. Acad. Sci. (Paris)*, 1966, **263B**, 819.

[ii] F. Auzel, *F.C.R. Acad. Sci. (Paris)*, 1966, **262**, 1016.

[iii] V. Ovsyankin and P.P. Feofilov, *Jetp Lett.*, 1966, **4**, 317.

[iv] S. Heer, O. Lehmann, M. Haase and H. U. Güdel, *Angew. Chem., Int. Ed. Engl.*, 2003, **42**, 3179.

[v] R. S. Niedbala, H. Feindt, K. Kardos, T. Vail, J. Burton, B. Bielska, S. Li, D. Milunic, P. Bourdelle and R. Vallejo, *Anal. Biochem.*, 2001, **293**, 22.

[vi] M. Seydack, *Biosens. Bioelectron.*, 2005, **20**, 2454.

[vii] M. Bass, A. Rapaport, H. Jennsen, *US Pat.*, 6654161, 2003.

[viii] E. Downing, L. Hesselink, J. Ralston and R. Macfarlane, *Science*, 1996, **273**, 1185.

[ix] A. Rapaport, J. Milliez, M. Bass, A. Cassanho and H. Jenssen, *J. Display Technol.*, 2006, **2**, 68.

[x] C. Strumpel, M. McCann, G. Beaucarne, V. Arkhipov, A. Slaoui, V. Svrcek, C. del Canizo and I.Tobias, *Sol. Energy Mater. Sol. Cells*, 2007, **91**, 238.

[xi] T. Trupke, M.A. Green and P. Würfel, *J. Appl. Phys.*, 2002, **92**, 4117.

[xii] B. S. Richards and A. Shalav, *IEEE Trans. Electron Devices*, 2007, **54**, 2679.

[xiii] A. Shalav, B. S. Richards and M. A. Green, *Sol. Energy Mater. Sol. Cells*, 2007, **91**, 829.

[xiv] A. O. Patil, A. J. Heeger and F. Wudl, *Chem. Rev.*, 1988, **88**, 183.

[xv] N. S. Sariciftci, L. Smilowitz, A. J. Heeger and F. Wudl, *Science*,1992, **258**, 1474.

[xvi] S.R. Bullock, B.R. Reddy, P. Vankateswarlu and S.K. Nash-Stevenson *J. Opt. Soc. Am.* , 1997, **14,** 553.

[xvii] B.R. Reddy, S.K. Nash-Stevenson and P. Vankateswarlu, *J. Opt. Soc. Am. B*, 1994, **11**, 923.
[xviii] X. Zou and H. Toratani, *J. Non-Cryst. Solids*, 1996, **201**, 37.

[xix] D.N. Patel, B.R. Reddy and S.K. Nash-Stevenson, *Opt. Mater.*, 1998, **10**, 225.

[xx] P. Muller, M. Wermuth and H.U. Güdel, *Chem. Phys. Lett.*, 1998, **290**, 105.

[xxi] R.M. Moses, J.P.R. Wells, H.G. Gallagher, T.P.J. Han, M. Yamada, N. Kodama and T. Yosida, *Chem. Phys. Lett.*, 1998, **286**, 291.

[xxii] S. Kuck and I. Sokólska, *Chem. Phys. Lett.*, 2000, **325**, 257.

[xxiii] L.B. Shaw, R.S.F. Chang and N. Djeu, *Phys. Rev. B*, 1994, **50**, 6609.

[xxiv] M. Malinowski, Z. Frukacz, M. Szuflinska, A. Wnuk, M. Kaczkan, *J. Alloys Comp.*, 2000, **300**, 389.

[xxv] E. De la Rosa, P. Salas, H. Desirena, C. Angeles, R. A. Rodriguez, *Appl. Phys. Lett.*, 2005, **87**, 241912.

[xxvi] W. Ryba-Romanowski, S. Golab, G. Dominiak-Dzik, P. Solarz and T. Lukasiewicz, *Appl. Phys. Lett.*, 2001, **79**, 3026.

[xxvii] J. C. Boyer, F. Vetrone, J. A. Capobianco, A. Speghini, M. Zambelli and M. Bettinelli, *J. Lumin.*, 2004, **106**, 263.

[xxviii] J. A. Capobianco, J. C. Boyer, F. Vetrone, A. Speghini, M. Bettinelli, *Chem. Mater.*, 2002, **14**, 2915.

[xxix] C. Michel and B. Raveau, *J. Solid State Chem.*, 1982, **43**, 73.

[xxx] C. Michel and B. Raveau, *J. Solid State Chem.*, 1983, **49**, 150.

[xxxi] A. Birkel, A. A. Mikhailovsky and A. K. Cheetham, *Chem. Phys. Lett.*, 2009, **477**, 325.

[xxxii] I. Etchart, A. Huignard, M. Bérard, M. N. Nordin, I. Hernández, R. J. Curry, W. P. Gillin and A. K. Cheetham*, J. Mater. Chem.*, 2010, **20**, 3989.

[xxxiii] H. M. Rietveld, J. Appl. Cryst., 1969, **2**, 65.

[xxxiv] R. Buisson and J.C. Vial, *J. Phys. Lett.*, 1981, **42**, L115.

[xxxv] E. Nakazawa, in: S. Shionoya, W. M. Yen (Eds.), Phosphor Handbook, CRC Press, Boca Raton, 1999, p. 101.

[xxxvi] R. S. Quimby and B. G. Aitken, *J. Non Cryst. Sol.*, 2003, **320**, 100.

[xxxvii] I. R. Martín, V. D. Rodríguez, V. Lavín and U. R. Rodríguez-Mendoza, *J. Alloys Comp.*, 1998, **275-277**, 345.

[xxxviii] J. C. Boyer, F. Vetrone, J. A. Capobianco, A. Speghini and M. Bettinelli, *Chem. Phys. Lett.*, 2004, **390**, 403.

[xxxix] R. Lisiecki, W. Ryba-Romanowski, T. Lukasiewicz, M. Mond and K. Petermann, *Laser Phys.*, 2005, **15**, 306.

[xl] Z. Wang, Y. Yin and D. Yuan, *J. Alloys Comp.*, 2007, **436**, 364.

[xli] I. R. Martin, V. D. Rodríguez, M. Morales, U. R. Rodríguez-Mendoza and V. Lavín, *J. Appl. Spectrosc.*, 1995, **62**, 865.

[xlii] P. J. Derén, J.-C. Krupa, *J. Alloys Comp.*, 2004, **380**, 362.

[xliii] L. Esterowitz, J. Noonan and J. Bahler, Appl. Phys. Lett., 1967, **10**, 126.

[xliv] R. K. Watts, *J. Chem. Phys.*, 1970, **53**, 3552.

[xlv] X. X. Zhang, M. Bass, B. H. T. Chai and R. E. Peale, *OSA Proceedings on Advanced Solid-State Lasers*, New Orleans, LA, February 1993 (in press).

[xlvi] C. B. Layne, W. H. Lowdermilk, and M. J. Weber, *Phys. Rev. B*, 1997, **16**, 10.

[xlvii] D. A. Zubenko, M. A. Noginov, V. A. Smirnov and I. A. Shcherbakov, *Phys. Rev. B*, 1997, 55, 8881.

[xlviii] I. Hernandez, R.H.C. Tan, J.M. Pearson, P.B. Wyatt and W.P. Gillin, *J. Phys. Chem. B*, 2009, **113**, 7474.